Documentation - Theory

SAR Processing

GAMMA REMOTE SENSING

Version 1.4 – March 2008

GAMMA *Remote Sensing AG, Worbstrasse 225, CH-3073 Gümligen, Switzerland*
tel: +41-31-951 70 05, fax: +41-31-951 70 08, email: gamma@gamma-rs.ch

Table of contents

List of acronyms

ALOS	Advanced Land Observing Satellite
AP	Alternating Polarization
ASAR	Advanced Synthetic Aperture Radar
CEOS	Committee on Earth Observation Satellites
DEOS	Department of Earth Observation and Space Systems
DLR	Deutsches Luft- und Raumfahrtzentrum
DORIS	Doppler Orbitography and Radiopositioning Integrated by Satellite
ENVISAT	ENVIronmental SATellite
EORC	Earth Observation Research Center
ERS	European Remote Sensing (Satellite)
ERSDAC	Earth Remote Sensing Data Analysis Center
ESA	European Space Agency
ESRIN	European Space Research Institute
FBAQ	Flexible Block Adaptive Quantization
FFT	Fast Fourier Transform
FM	Frequency Modulated
GFZ	Geoforschungszentrum
IM	Image Mode
IMU	Inertial Motion Unit
JERS	Japanese Earth Resources Satellite
MLBF	Multi-Look Beat Frequency
MLCC	Multi-Look Cross Correlation
PAF	Processing and Archiving Facility (D = Germany I = Italy, UK =United Kingdom)
PALSAR	Phased Array L-band Synthetic Aperture Radar
PRF	Pulse Repetition Frequency
SAR	Synthetic Aperture Radar
SRTM	Shuttle Radar Topography Mission
SLC	Single Look Complex
SLR	Single Look Complex
SNR	Signal to Noise Ration
UTC	Coordinated Universal Time

1. Introduction

The expression "SAR processing" refers to the generation of a SAR image starting from raw data. The transformation of data from the raw format (also referred to as level 0 as in the case of ERS and ENVISAT ASAR data or 1.0 as in the case of PALSAR) to Single Look Complex (SLC) format (also referred to as level 1 as in the case of ERS and ASAR or 1.1 as in the case of PALSAR) basically requires the matched filtering of the raw data in range and in azimuth with corresponding reference functions. Although the two directions, i.e. range and azimuth, are not independent from each other, processing of a SAR image consists in separate actions on the range spectrum and on the azimuth spectrum. Figure 1 illustrates with a simplified block diagram the core of SAR processing using a Range/Doppler algorithm.

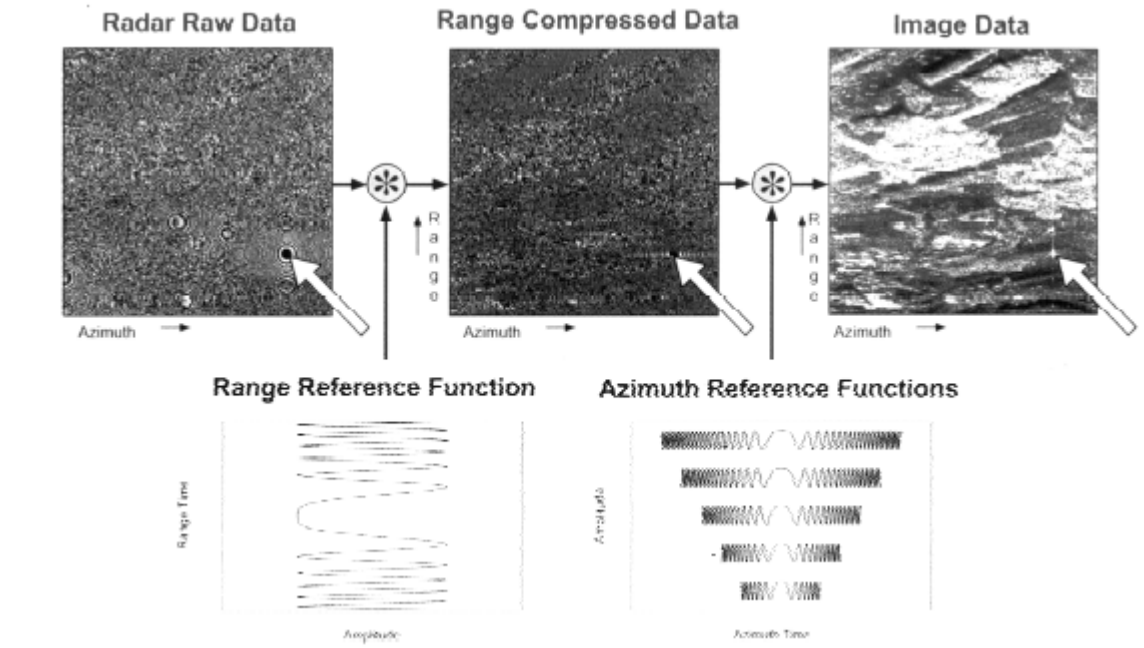

Figure 1. Simplified scheme of a Range/Doppler algorithm (from DLR-Nachrichten, Heft 86, June 1997, p 42).

Before proceeding to the matched filtering, a set of pre-processing steps can be applied. Data should be checked for errors such as missing lines. If a long strip of data should be processed, it is possible to generate a single image by concatenating consecutive frames; in this case it is fundamental that range positions are all aligned. If data are to be processed interferometrically or geocoded, the orbit state vectors should be improved if possible or necessary. These aspects will be treated in Sections 2. Sections 3 and 4 illustrate the derivation of range and azimuth spectrum respectively. In Section 5 range compression is presented. Section 6 and 7 describe the analogous processing to be applied in the azimuth direction. In addition, Section 7 illustrates the approaches to radiometrically calibrate the SAR image in SLC format obtained after range and azimuth compression. In Section 8 multi-looking is discussed together with the conversion of geometry from slant-range to ground-range. A list of relevant publications on SAR processing is provided at the end of this document.

The flowchart in Figure 2 shows schematically the SAR processing phases including for each phase the individual steps. Input and output data are also illustrated.

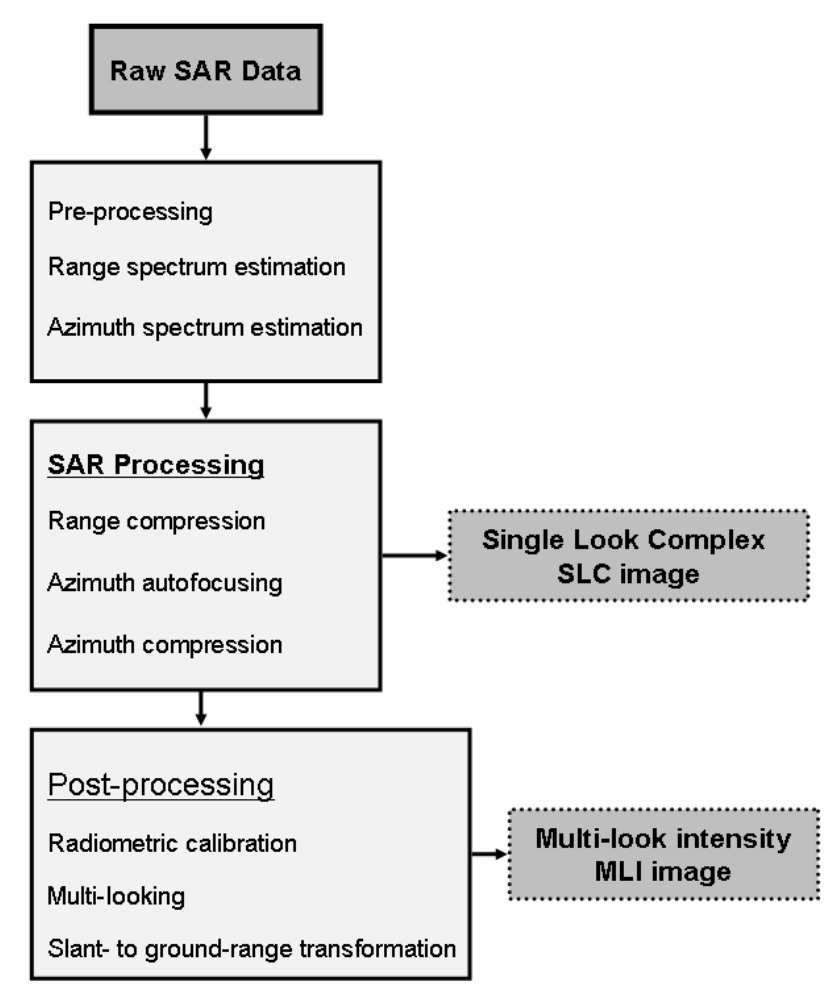

Figure 2. SAR processing scheme.

2. Pre-processing

2.1. Concatenation and conditioning

Missing lines occur for ERS raw data only. ERS raw data from the different PAFs often has missing data lines, which is basically due to transmission problems. In some cases this problem can be so severe that literally hundreds of lines are missing from the file. If only a few lines are missing, it is almost impossible to tell if examining the multi-look intensity image produced from the file. But for interferometric applications, if only one line is missing, interferometric correlation will be almost completely lost between images, a completely unacceptable situation. A possible way to correct for missing lines is to introduce a number of fictious lines with zeros.

When several consecutive frames are available, it is possible to generate a single long stripe of raw data by concatenating the data. Since in some cases (e.g. ERS and JERS-1) the range gate position (i.e. the slant range to the first line) changes along the orbital track, concatenation of several frames of raw data would suffer of unaligned iso-range values if not compensated for. In the case of ERS the range gate position changes with an interval of 30 seconds, which means that every second image frame is misaligned in range.

2.2. Manipulation of orbital state vectors

State vectors are typically provided with the image data by the data processing facilities and include instant position and velocity of the satellite components expressed in the Earth-centered Cartesian coordinate system. In some cases the number of state vectors provided with the image data might be insufficient for correct processing or cover an area that is too small compared to the length of the image to be processed. For this reason additional state vectors need to be introduced by respectively interpolation of the available state vectors and orbit propagation. Another problem, which in particular concerns ERS, ENVISAT, JERS-1 and RADARSAT-1 data, is that the orbit data provided with the image data file is not precise enough. This is a drawback for example when determining the interferometric phase or image geocoding. Precise orbit for ERS and ENVISAT can be obtained from several sources listed below. No precise orbit data is available for JERS-1 and RADARSAT-1.

2.2.1. DELFT orbits

The Department of Earth Observation and Space Systems (DEOS) at the Technical University of Delft provides highly precise orbits for ERS-1, ERS-2 and ENVISAT, in support of altimetric and interferometric SAR research. The DELFT orbit data (and the software that supports their manipulation) can be obtained from the DEOS website http://www.deos.tudelft.nl/ers/precorbs. The orbits are distributed as files (*.ODR) for ERS-1, ERS-2, and ENVISAT. The ODR data sets have significant overlap and cover approximately 3 to 5 days of orbital data. The list of ODR files available at DEOS including the start and end date for each ODR file is available in the text file *arclist*. Details on the DELFT package and state vector format are available at the DEOS website.

2.2.2. PRC Precision Orbits

PRC orbits are made available for ERS-1 and ERS-2 by ESA. The precise orbit results from a data reduction process in which all available tracking data and most accurate correction, transformation and dynamical models are taken into account and in which high level numerical procedures are applied. Processing is carried out by D-PAF and GFZ Potsdam. More information is available at the dedicated website http://earth.esa.int/services/pg/pgersorbprc.xml.

The PRC data are available from an ftp server in Germany with a delay of about 1 month after data acquisition by ERS. Apply to the ESA Helpdesk at ESA ESRIN to get an account to access these data (eohelp@esa.int). The PRC data contain the position and velocity of the sensor in both body-fixed and inertial coordinates. Sensor attitude data is also kept with the state vectors. PRC data are available with a delay of about 1 month and cover a period of about 5-7 days each. The PRC filenames contain the date of the first state vector and the starting orbit number.

The PRC files consist of 130 byte text records containing the Julian date and time of the state vector data, the position, velocity and attitude of the ERS sensor, and data quality information. State vectors are given on 30 second intervals. The format of the PRC data file records is described in an ESA document available from the abovementioned ESA ESRIN website.

2.2.3. DORIS precision orbits

Precise orbits for ENVISAT are determined from Doppler shift data measured by the DORIS instrument. The precise orbit reconstruction is the most accurate orbit estimate produced from the DORIS data. The file is used during ground processing and is updated once per day.

A file containing DORIS precision orbits consists of 129 byte text records containing the date, time, offset between UTC and UT1, orbit, position, and velocity, and data quality information. State vectors are given on 60 second intervals.

The format of the DORIS data file records is described in an ESA document available from http://envisat.esa.int/dataproducts/asar/CNTR2-9-3.htm. Access to the DORIS data is via a request to the ESA ESRIN Helpdesk (eohelp@esa.int). Data are available on an ESA ftp site and are updated with 4-6 weeks delay from acquisition. The orbit data are arranged in files covering a full day and extending to the previous day by a couple of hours. Data are available starting July 22, 2002. For previous dates the DELFT orbits should be considered. The DORIS orbits file name starts with DOR_VOR_AXVF-. Then date and time of processing, start date and time of the orbit data, end date and time of the orbit data follow. Format for the date is yyyymmdd. Format for the time is hhmmss (e.g. DOR_VOR_AXVF-P20020906_120800_20020722_215528_20020724_002328). [

3. Range Spectrum Estimation

The range spectrum gives a representation of the spectral properties of a dataset across range, thus including range chirp, noise and properties of the scattering objects. Figure 3 shows an example of a range spectrum for a RADARSAT-1 SAR image frame. The spectrum can be retrieved by applying a Fast Fourier Transform (FFT) to the raw dataset. The range spectrum is useful for estimating the signal-to-noise ratio, SNR, of the final image. Typically, the spectrum extends over about 80 percent of the digitized bandwidth. The SNR estimate is obtained by comparing the average level chirp bandwidth to the level in the noise only region. This estimate is then used for radiometric compensation of the antenna pattern gain used for calibration of the SAR image, since the antenna gain correction applies only to the signal and not the noise fraction of the SAR image.

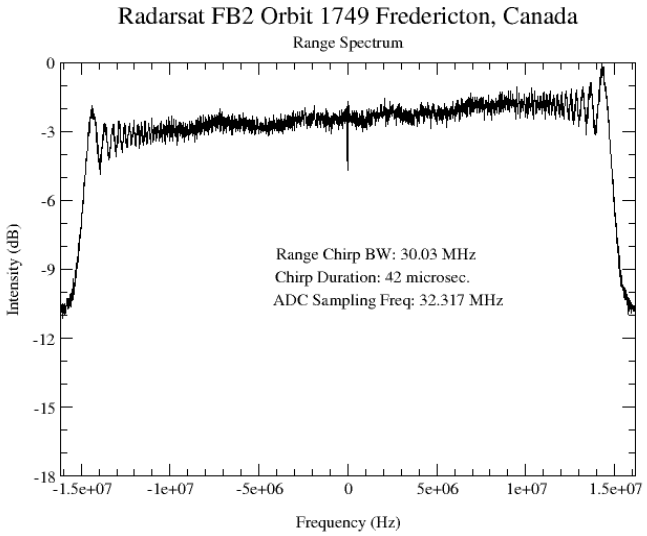

Figure 3. Range spectrum of a RADARSAT-1 SAR data set.

4. Azimuth Spectrum Estimation

The azimuth spectrum of a SAR dataset contains the Doppler information that will be exploited in the azimuth compression to improve the resolution of the dataset along-track. In an ideal case, the Doppler frequency of a target decreases almost linearly passing through 0 at the point of closest approach. The Doppler frequency of points at center of the antenna beam i.e. at the point of closest approach is called the Doppler Centroid. Under ideal conditions the Doppler centroid is zero. Non-zero Doppler Centroid and variation of Doppler along track can however occur and have to be considered when processing a raw dataset to form a SAR image.

Non-zero Doppler conditions are due to the presence of squint. Squint means that the look direction of the antenna is not perpendicular to the flight direction. Figure 4 illustrates the case of squint by showing the squint look direction, i.e. the look direction under squinting conditions. The angle α represents the squint angle.

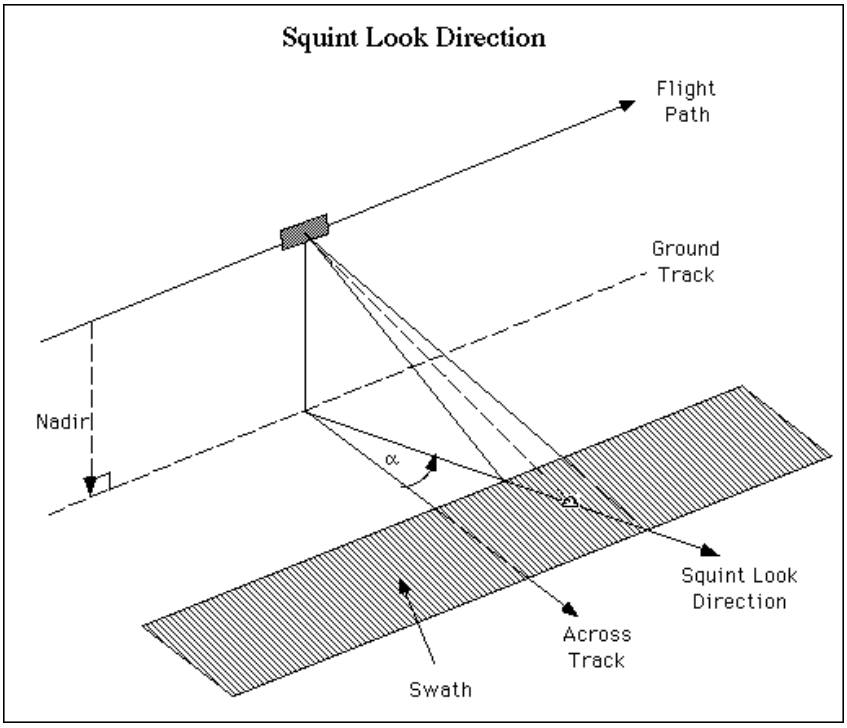

Figure 4: Illustration of squint angle (from http://www.asf.alaska.edu/reference/reference_docs.html)

The center of the side-looking antenna beam may not be exactly broadside to the flight track of the radar for a number of reasons including inaccurate pointing information, winds (aircraft), or other electrical or mechanical factors. In this case the antenna is squinted with respect to the direction it should have to generate a zero-Doppler Centroid.

Doppler variation along track is primarily a result of the different contribution of the Earth's velocity to the total earth body fixed velocity of the platform. The spacecraft nadir track would be a great circle if Earth did not rotate. Earth rotation makes the effective body fixed spacecraft velocity different from the inertial velocity. Assuming that the radar antenna is oriented along the spacecraft inertial velocity, it results in an effective yaw angle for the antenna that varies from 0° to 4° (see Figure 5).

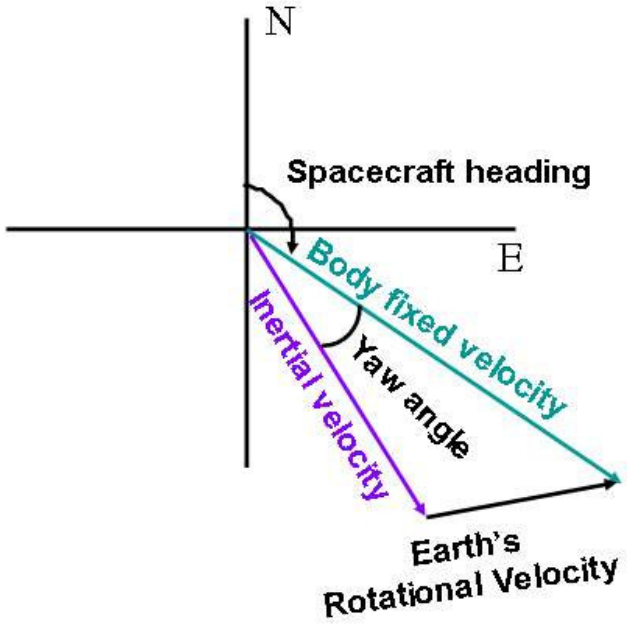

Figure 5. Inertial velocity as a result of body fixed velocity (i.e. velocity of the platform) and Earth's rotational velocity. The inertial velocity is the relative velocity of the platform with respect to the point on the ground.

In the presence of a squint angle θ_s it can be demonstrated that the instantaneous slant range distance, R, for a position x along track is given by:

$$R(x) \cong R(0) + \frac{x^2}{2R(0)} - x\sin\theta_s \tag{1}$$

where x=0 corresponds to the closest approach position.

The instantaneous Doppler frequency $f_d(t)$ and the variation of it in time (i.e. the chirp rate) $f_r(t)$ as a function of time, i.e. range, are then given by:

$$f_d(t) \cong -\frac{2}{\lambda}\frac{dR}{dt} = \frac{-2v_{rel}}{\lambda} + \frac{2v_{rel}\sin\theta_s}{\lambda} \tag{2}$$

$$f_r(t) \cong \frac{d}{dt} f_d(t) = -\frac{2v_{rel}^2}{\lambda R(0)} \tag{3}$$

From (2) we see that at the point of closest approach, for which we have t=0, the Doppler frequency is non-zero in case of squint. The Doppler frequency rate is related to the square of the radial component of the velocity (see (3)).

Accurate matched filtering of the radar echoes requires the Doppler history, including the ambiguities due to squinting of the antenna boresight away from perpendicular to the SAR track (zero-Doppler) line. The concept of Doppler ambiguity and the way to resolve the ambiguity will be further explained in Section 4.1. Techniques that allow taking into account variations of Doppler along track are described in Section 6.

4.1. Doppler Ambiguity Resolution

The simplest method to determine the azimuth spectrum is to apply a FFT and analyze the representation of the signal in the frequency domain. When the center of the side-looking antenna beam is not exactly broadside to the flight track of the radar, the Doppler frequency history of the target does not pass through zero at the point of closest approach. In this case the Doppler centroid is non-zero and the spectrum is shifted. The offset from the zero-Doppler case can be of the order of several thousand Hz depending on the amount of squint. In such cases an ambiguity problem can occur.

Due to the fact that the radar is a sampled data system, i.e. the SAR acquires echoes at the rate of the pulse repetition frequency (PRF), the azimuth spectrum is periodic in the interval (–PRF/2, +PRF/2). If the Doppler centroid is very large, aliasing can occur, i.e. the Doppler frequency estimated from the azimuth spectrum is shifted with respect to the true Doppler frequency by an integer number of the PRF. This is called azimuth ambiguity.

This means that the analysis of the azimuth spectrum is not sufficient for setting the Doppler Centroid and the Doppler history but rather some other method must be used to determine an unambiguous value of the Doppler centroid apart from simple analysis of the azimuth spectrum.

Several methods exist for estimating the Doppler ambiguity. The most reliable method would be to use accurate data on the spacecraft attitude if available to estimate the squint angle from which the Doppler frequency information can be retrieved.

The ERS-1 and ERS-2 SAR platforms employ yaw steering of the radar in order to maintain the Doppler centroid of the data within 1/2 of the PRF. In this case an estimate of the Doppler centroid is unambiguous because the Nyquist criterion for sampling of band-limited signals is satisfied. A more general form of the Nyquist criteria states that as long as the bandwidth of the signal is less than the sampling rate (the PRF), the original signal can be recovered if the correct multiple of the sampling frequency is known. As it turns out, the pointing algorithm for ERS makes errors in the southern hemisphere such that the actual Doppler centroid is 1 to 2 multiples of the PRF away from baseband.

Both RADARSAT-1 and JERS-1 do not employ yaw steering to control the PRF and so the centroid is a function of the sensor latitude. Large amounts of yaw in the SAR data not only complicates processing, but degrades image resolution. Lack of precise yaw steering will also lead to degraded interferometry results because optimal correlation of passes requires that a point on the ground be viewed from exactly the same angle for repeated passes.

The SAR used during the Shuttle Radar Topography Mission (SRTM) had sufficient accuracy to estimate the centroid directly. In addition it had an on-board Doppler tracker that kept the centroid locked to zero. Current generation of SAR sensors (ENVISAT ASAR, ALOS PALSAR, and RADARSAT-II) has improved pointing capability and knowledge.

As mentioned before, when we have the case of large squint angles, exceeding the beamwidth of the SAR antenna, aliasing of the Doppler occurs. Processing the SAR with an aliased value of the centroid means that the estimate of the range migration rate of targets in the image is incorrect. In other words a target is positioned at a wrong position. Failing direct measurement techniques, the most reliable method to obtain unambiguous Doppler estimates

is to measure uncompensated range migration determined by correlation of images processed from different parts of the Doppler spectrum. For these algorithms to work well, the fractional bandwidth of the SAR should be large and the scene relatively devoid of features.

In (Wong et al., 1996) two algorithms are described to determine an unambiguous estimate of the Doppler centroid. A first algorithm, called the Multi-Look Cross Correlation algorithm (MLCC), estimates the Doppler centroid for different bands of the range chirp bandwidth. The estimate of the centroid is performed by evaluating the complex correlation between echoes. The phase of the correlation coefficient is directly proportional to the centroid. Examining the shift in centroid as a function of frequency yields an unambiguous estimate of the centroid. A second algorithm, called the Multi-Look Beat Frequency (MLBF), again uses the idea of using different range looks, but rather than using the correlation coefficient, the spectrum of the product of the range looks is evaluated. The signal phase from different complex range looks is used to obtain an unambiguous estimate of the Doppler centroid. This algorithm works best in regions with point targets such as suburban and urban regions. While regions of high contrast can introduce errors in the MLCC algorithm, processing of a large data block reduces this sensitivity.

4.2. Fractional Doppler Centroid Estimation

Once the correct number of ambiguities has been computed, the fractional part of the Doppler centroid can be estimated using either the line to line complex cross-correlation method (Madsen, 1989) or by finding the centroid of the azimuth power spectrum using an incoherent summation of azimuth spectra (Li et al., 1985). Both of these approaches provide reliable estimates of the centroid modulo the PRF, although with the first one it is possible to take into account variations of the Doppler frequency across range.

The centroid of ERS and ENVISAT ASAR data is quite constant across the swath so that the azimuth spectrum approach works well (see Figure 6). It should be however noticed that large variations occur for ERS-2 since 2001 when the attitude started being controlled in the so-called Zero Gyro mode. RADARSAT-1, JERS-1 and PALSAR often have a large squint angles causing the centroid to change more than 1/2 PRF across the swath (see Figure 7). In this case it is necessary to use the complex correlation method.

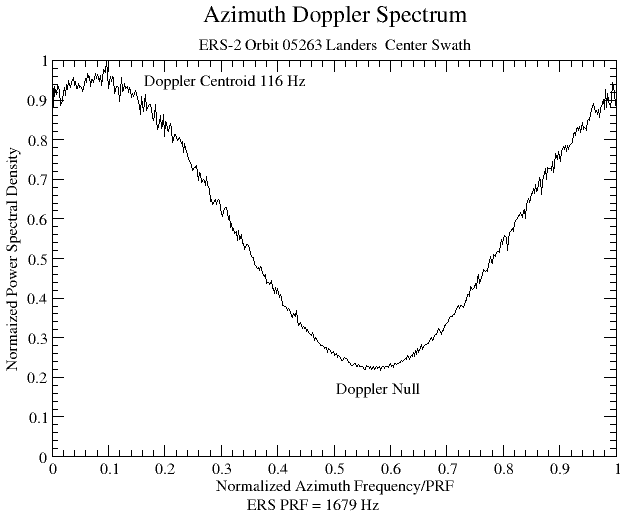

Figure 6. Azimuth spectrum of an ERS-2 SAR data set.

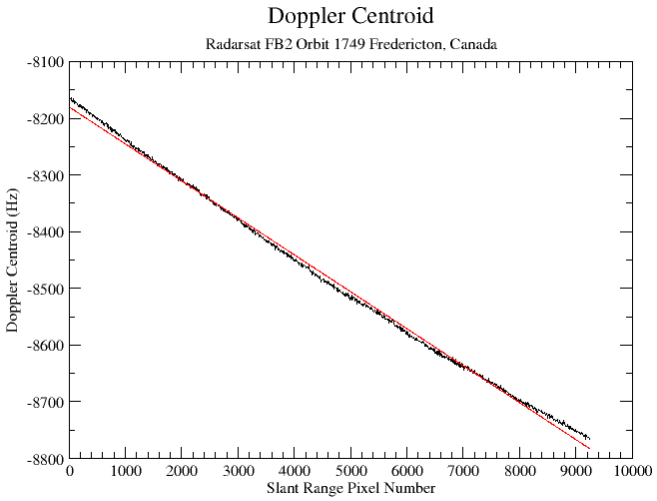

Figure 7. Doppler centroid as a function of range position in a RADARSAT-1 image. The red line indicates the linear fit to the measurement (black line).

5. Range Compression / Azimuth Prefilter

As the radar travels along the flight track, the transmitted pulses are linear FM modulated chirp signals with a large time-bandwidth product. Range compression applies a matched filter in range to the recorded data as illustrated in Figure 1. This step recovers the full range resolution inherent in the range chirp bandwidth by compressing all the energy distributed over the chirp duration into an as narrow possible time window consistent with window function weighting used in processing.

Range compression algorithms partly depend on the sensor. They all work similarly except for variations in compensation for backscatter variation along-track and across the swath which is sensor dependent and has to be taken into account. All programs estimate the raw data histogram, and data statistics, including the mean of each channel, standard deviation, and in the case of IQ data, the correlation between the I and Q channels.

An important parameter for determining the sidelobe level and resolution of the range compressed data is the window applied to the range reference function. One type of window is the Kaiser-Bessel window as the weighting function. The relationship between the resolution and sidelobe level can be changed by adjusting the window parameter beta. The default value of beta is 2.12 which leads to sidelobes of approximately -25 dB. This window is discussed in most standard texts on digital signal processing such as (Oppenheim et al., 1975).

Prior to range compression it is possible to decimate the data in azimuth by pre-filtering around the Doppler centroid. This might be desirable if a quick-look survey product is desired. This step can also be performed after range compression. It is not necessary in fact to estimate the Doppler centroid before range compression unless secondary Doppler range correction is required, as in the case of RADARSAT-1. Nevertheless it is strongly recommended that the Doppler estimation is performed before range compression.

Figure 8 gives an example of a range-compressed image together with the final product obtained after azimuth compression as well. In the range compressed image point targets are

clearly visible as elongated features. Other targets are not recognizable. Figure 9 shows a detail for a point target after range compression.

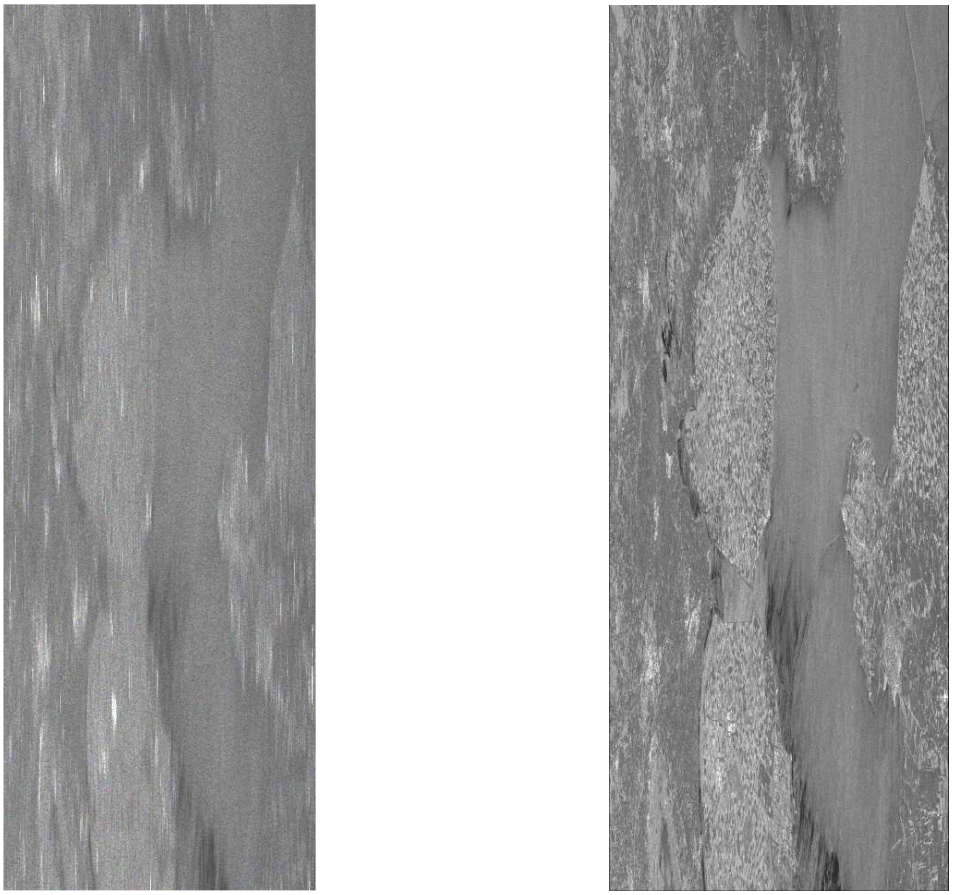

(a) (b)

Figure 8. Range compressed image (a) and detected SLC (b) for an ERS-2 image of Flevoland, the Netherlands. The azimuth direction corresponds to the vertical direction.

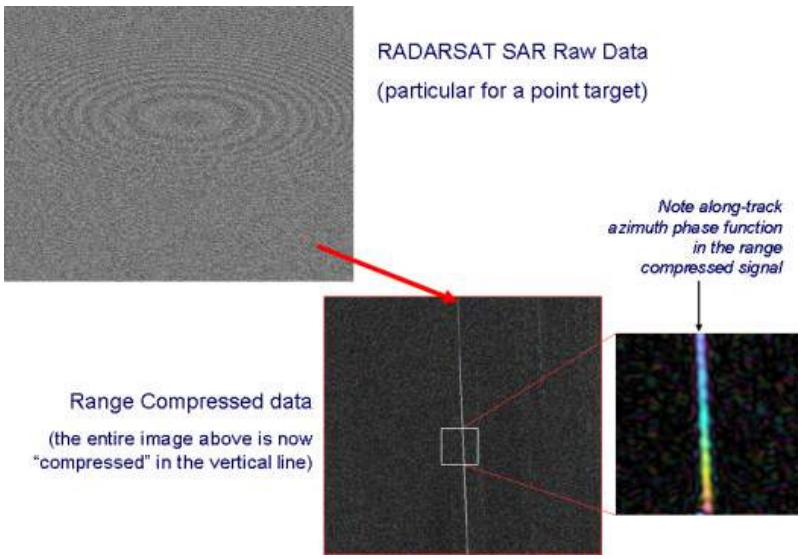

Figure 9. Detail view for a point target in a RADARSAT dataset. In the raw dataset the point target appears in the form of circles, due to the chirp in range and azimuth. The range compressed signal shows variation along the azimuth direction (vertical).

6. Azimuth auto-focusing

Matched filtering of the Doppler history for points on the ground requires precise knowledge of the range and velocity of radar platform. Only in this way will the processed image focus properly. Errors in along-track velocity and acceleration of the radar lead to blurred images. Nominally the radar does not fly along a straight path. Efficient azimuth processing requires that the flight track follows a smooth curve, in our case a curve parallel to the approximating sphere to earth surface below the radar.

Deviations from this smooth curve as occurs for airborne SAR causes severe defocusing. To overcome this, precise measurement of the aircraft motion with an Inertial Motion Unit (IMU) is required. These data are processed to obtain the precise position and velocity of the radar antenna which is the reference phase center of the radar. Displacements of the antenna from the nominal reference track can be used to estimate phase and amplitude corrections on the data in order to obtain an approximation of what the data would have been, had the aircraft actually flown the nominal track. In this way motion compensation of the SAR data is achieved.

7. Azimuth compression

For azimuth compression of range compressed data the range-Doppler algorithm is typically used. The range compressed data are divided into along-track patches of selectable length. Range migration of the range compressed data is required since each point in the image follows a parabolic range trajectory. The algorithm is based on the idea that all points at a particular Doppler frequency will have to be migrated by the same amount at a particular range. This is why in the algorithm the migration is done after an azimuth FFT of the data is carried out. A 9-point sinc interpolation kernel is used to perform the interpolation. After migration, an azimuth matched filter derived from the range history of a point target is applied. The range history is calculated without approximation and updated for every range bin. The result of azimuth compression can be seen in Figures 1 and 8.

After range and azimuth compression, the magnitude of the resulting image is not uniform all over the scene but suffers from different effects related e.g. to the pattern of the antenna diagram, the longer traveling path of a wave in far range compared to near range etc. To adjust the magnitude level of the image, relative calibration is needed. Relative calibration of an image takes into account the antenna pattern in range, the variation in slant range, and the variation in length of the azimuth reference function, the interpolation window function, the ground-surface projection for a horizontal surface. An additional factor needs to be then considered for absolute radiometric calibration. The antenna pattern is only important for radiometric calibration and has no effect on the interferometric phase or coherence.

A calibrated SLC can be either in the *sigma0* or in the *gamma0* form. In the *sigma0* case the SLC image intensity (SQR(re)+SQR(im)) corresponds to the backscattering coefficient σ^o (normalized to the horizontal ground surface). In the case of *gamma0* the SLC image intensity (SQR(re)+SQR(im)) corresponds to the backscattering coefficient γ^o, which is related to σ^o by

$$\gamma^o = \sigma^o / \cos\theta \tag{4}$$

with θ being the incidence angle of the horizontal surface.

8. Multi-looking

SAR images have coherent speckle noise that arises from the coherent interference of signals scattered from different parts of the radar resolution element. This noise is suppressed by the incoherent summation of statistically independent images of the scene. Each of the images formed from the different Doppler bands are independent because they view the scene with different aspect angles. Further suppression of speckle noise can be achieved by local incoherent spatial averaging of pixels at cost of reduced spatial resolution.

Figure 10 shows the effect of spatial multi-looking of an ERS-2 SAR image. The detected intensity of the SLC on the left side presents significant speckle. This has been partly filtered out in the upper image on the right with a multi-look factor of 5 in azimuth. With a stronger multi-look (4 in range and 20 in azimuth), noise reduction has been more powerful but there has also been a significant loss in resolution.

(a)

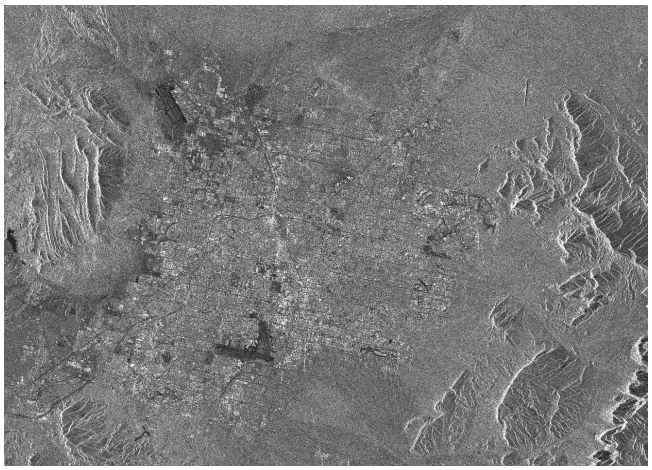

(b)

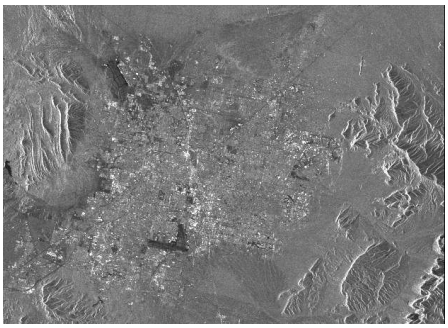

(c)

Figure 10. Intensity of SLC (a), 1x5 multi-looked intensity image (b), 4x20 multi-looked intensity image (c). Data: ERS SLC over Las Vegas, dimensions: 9000 lines, 2500 samples.

References

Elachi, C., Spaceborne Radar Remote Sensing: Applications and Techniques. New York: IEEE Press, 255, 1987.

Li, F. K., Held, D. N., Curlander, J. C. and Wu, C., "Doppler parameter estimation for spaceborne synthetic-aperture radars," IEEE Transactions on Geoscience and Remote Sensing, vol. GE-23, pp. 47-56, 1985.

Madsen, S. N., "Estimating the Doppler centroid of SAR data," IEEE Transactions on Aerospace and Electronic Systems, vol. 25, pp. 134-140, 1989.

Oppenheim, A. V., and Schafer, R. W., Digital Signal Processing, 2nd Edition ed. Englewood Cliffs, NJ: Prentice-Hall, 1975.

Wong, F. and Cumming, I. G., "A combined SAR Doppler centroid estimation scheme based upon signal phase," IEEE Transactions on Geoscience and Remote Sensing, vol. 34, pp. 696-707, 1996.

Bibliography on SAR Processing

Bamler, R., and Runge, H., "PRF-ambiguity resolving by wavelength diversity," IEEE Transactions on Geoscience and Remote Sensing, vol. 29, 6, pp. 997-1003, 1991.

Bamler, R., "A comparison of Range-Doppler and wavenumber domain SAR focusing algorithms," IEEE Transactions on Geoscience and Remote Sensing, vol. 30, 4, pp. 706-713, 1992.

Cafforio, C., Prati, C., and Rocca, F., "SAR data focusing using seismic migration techniques," IEEE Transactions on Aerospace and Electronic Systems, vol. 27, 2, pp. 194-206, 1991.

Carrara, W. G., Goodman, R. S., and Majewski, R. M., Spotlight Synthetic Aperture Radar - Signal Processing Algorithms. Boston: Artech House, 555, 1995.

Cumming, I. G., and Wong, F. H., Digital processing of synthetic aperture radar data. Norwood, MA: Artech House, Inc., 2005.

Curlander, J. C., and McDonough, R. N., Synthetic Aperture Radar: Systems and Signal Processing. New York: John Wiley & Sons, Inc., 1991.

Davidson, G. W., and Cumming, I. G., "Signal properties of spaceborne squint-mode SAR," IEEE Transactions on Geoscience and Remote Sensing, vol. 35, 3, pp. 611-617, 1997.

Davidson, G. W., Cumming, I. G., and Ito, M. R., "A chirp scaling approach for processing squint mode SAR data," IEEE Transactions on Geoscience and Remote Sensing, vol. 32, 1, pp. 121-133, 1996.

Elachi, C., Spaceborne Radar Remote Sensing: Applications and Techniques. New York: IEEE Press, 255, 1987.

Franceschetti, G., and Schirinzi, G., "A SAR Processor Based on Two-Dimensional FFT Codes," IEEE Transactions on Aerospace and Electronic Systems, vol. 26, 2, pp. 356-365, 1990.

Franceschetti, G., and Lanari, R., Synthetic aperture radar processing. Boca Raton, FL: CRC Press, 1999.

Jin, M. Y., and Wu, C., "SAR correlation algorithm which accommodates large-range migration," IEEE Transactions on Geoscience and Remote Sensing, vol. GE-22, 6, pp. 592-597, 1984.

Kay, S. M., Fundamentals of Statistical Signal Processing: Estimation Theory. New Jersey: Prentice Hall, 1993.

Laur, H., Bally, P., Meadows, P., Sanchez, J., Schaettler, B., Lopinto, E., and Esteban, D., "ERS SAR CALIBRATION - Derivation of the Backscattering Coefficient Sigma-Nought in ESA ERS SAR PRI Products," European Space Agency, ESA ESRIN Technical Note Issue 2, Rev. 5b, 1998.

Lavalle, C., "The Sinc Interpolation in the Impulse Response Function Analysis," Proceedings of IGARSS'92, Houston, Texas, 26-29 May, 1992, pp. 842-844, 1992.

Li, F. K., Held, D. N., Curlander, J. C., and Wu, C., "Doppler parameter estimation for spaceborne synthetic-aperture radars," IEEE Transactions on Geoscience and Remote Sensing, vol. GE-23, pp. 47-56, 1985.

Madsen, S. N., "Estimating the Doppler centroid of SAR data," IEEE Transactions on Aerospace and Electronic Systems, vol. 25, 2, pp. 134-140, 1989.

Moreira, A., "Real-time synthetic aperture radar (SAR) processing with a new subaperture approach," IEEE Transactions on Geoscience and Remote Sensing, vol. 30, 4, pp. 714-722, 1992.

Moreira, A., and Huang, Y., "Airborne SAR processing of highly squinted data using a chirp scaling approach with integrated motion compensation," IEEE Transactions on Geoscience and Remote Sensing, vol. 32, 5, pp. 1029-1040, 1994.

Moreira, A., Mittermayer, J., and Scheiber, R., "Extended chirp scaling algorithm for air- and spaceborne SAR data processing in Stripmap and ScanSAR imaging modes," IEEE Transactions on Geoscience and Remote Sensing, vol. 34, 5, pp. 1123-1136, 1996.

Oliver, C., and Quegan, S., Understanding Synthetic Aperture Radar Images. Boston: Artech House, 1998.

Oppenheim, A. V., and Schafer, R. W., Digital Signal Processing, 2nd Edition ed. Englewood Cliffs, NJ: Prentice-Hall, 1975.

Quegan, S., "Interpolation and Sampling in SAR Images," IEEE Transactions on Geoscience and Remote Sensing, vol. 28, 4, pp. 641-646, 1990.

Raney, R. K., "Radar Fundamentals: Technical Perspective," in Principles and Applications of Imaging Radar, vol. 2, Manual of Remote Sensing, Henderson, F. M., and Lewis, A. J., Eds., 3rd ed. New York: John Wiley & Sons, pp. 9-130, 1998.

Raney, R. K., Runge, H., Bamler, R., Cumming, I. G., and Wong, F. H., "Precision SAR processing using chirp scaling," IEEE Transactions on Geoscience and Remote Sensing, vol. 32, 4, pp. 786-799, 1994.

Wong, F., and Cumming, I. G., "A combined SAR Doppler centroid estimation scheme based upon signal phase," IEEE Transactions on Geoscience and Remote Sensing, vol. 34, 3, pp. 696-707, 1996.